CANCER RESEARCH COMMUNICATIONS

AACR American Association for Cancer Research

RESEARCH ARTICLE https://doi.org/10.1158/2767-9764.CRC-23-0097 OPEN ACCESS

Exploring the Onset and Progression of Prostate Cancer through a Multicellular Agent-based Model

Margot Passier[1,2], Maisa N.G. van Genderen[1], Anniek Zaalberg[3], Jeroen Kneppers[3], Elise M. Bekers[4], Andries M. Bergman[3,5], Wilbert Zwart[1,2,3], and Federica Eduati[1,2]

ABSTRACT

Over 10% of men will be diagnosed with prostate cancer during their lifetime. Arising from luminal cells of the prostatic acinus, prostate cancer is influenced by multiple cells in its microenvironment. To expand our knowledge and explore means to prevent and treat the disease, it is important to understand what drives the onset and early stages of prostate cancer. In this study, we developed an agent-based model of a prostatic acinus including its microenvironment, to allow for *in silico* studying of prostate cancer development.

The model was based on prior reports and in-house data of tumor cells cocultured with cancer-associated fibroblasts (CAF) and protumor and/or antitumor macrophages. Growth patterns depicted by the model were pathologically validated on hematoxylin and eosin slide images of human prostate cancer specimens. We identified that stochasticity of interactions between macrophages and tumor cells at early stages strongly affect tumor development. In addition, we discovered that more systematic deviations in tumor development result from a combinatorial effect of the probability of acquiring mutations and the tumor-promoting abilities of CAFs and macrophages. *In silico* modeled tumors were then compared with 494 patients with cancer with matching characteristics, showing strong association between predicted tumor load and patients' clinical outcome. Our findings suggest that the likelihood of tumor formation depends on a combination of stochastic events and systematic characteristics. While stochasticity cannot be controlled, information on systematic effects may aid the development of prevention strategies tailored to the molecular characteristics of an individual patient.

Significance: We developed a computational model to study which factors of the tumor microenvironment drive prostate cancer development, with potential to aid the development of new prevention strategies.

Introduction

Prostate cancer is generally diagnosed at late age, with 75% of all cases found in men over 65 years old (1, 2), while the formation of precursor neoplastic lesions is initiated years earlier (3). While localized prostate cancer can be cured, metastatic disease cannot, and its treatment is a clinical challenge (4, 5). Currently, prostate cancer is the second most diagnosed cancer and the second leading cause of cancer deaths in men globally (1). Studying the onset and early development of prostate cancer improves our understanding of this disease and could aid the development of new treatment strategies to prevent disease progression and to improve clinical care for patients with prostate cancer (6–10).

Prostate cancer generally initiates in the prostatic acini. In a normal acinus, the epithelium is highly organized with a bilayer of basal and luminal cells separated from the underlying stroma by the basement membrane. During the premalignant prostatic intraepithelial neoplasia (PIN) stage, luminal cells start to hyperproliferate (11, 12). Eventually, this can lead to the disruption of the basal cell layer and breakdown of the basement membrane, which is a prerequisite for the invasion of tumor cells into the tumor microenvironment (TME; refs. 11, 4), allowing cancer cells to metastasize (13, 14).

Prostate cancer is assumed to originate from mutations that confer a proliferative advantage to the transformed cells (15, 16). The accumulation of mutations is essential for the progression toward the malignant disease, and prostate cancer is characterized by a high heterogeneity of tumor cells (11, 4), with clonal selection shaping tumor evolution (17). Fibroblasts normally contribute to maintenance of the healthy homeostasis in the prostate (18–20). However, when in contact with neoplastic cells, they can differentiate into cancer-associated-fibroblasts (CAF; ref. 18). CAF differentiation can already occur in early premalignant stages, potentially contributing to the development

[1]Department of Biomedical Engineering, Eindhoven University of Technology, Eindhoven, the Netherlands. [2]Institute for Complex Molecular Systems, Eindhoven University of Technology, Eindhoven, the Netherlands. [3]Division of Oncogenomics, Oncode Institute, The Netherlands Cancer Institute, Plesmanlaan, Amsterdam, the Netherlands. [4]Division of Pathology, The Netherlands Cancer Institute, Amsterdam, the Netherlands. [5]Division of Medical Oncology, Netherlands Cancer Institute, Plesmanlaan, Amsterdam, the Netherlands.

Corresponding Authors: Federica Eduati, Eindhoven University of Technology, Eindhoven 5644PG, the Netherlands. Phone: +31 40 247 5939; E-mail: f.eduati@tue.nl; Andries M. Bergman, a.bergman@nki.nl; and Wilbert Zwart, w.zwart@nki.nl

doi: 10.1158/2767-9764.CRC-23-0097

and progression of prostate cancer by stimulating tumor cell proliferation (21) and migration (22, 23) and by altering the surrounding extracellular matrix (ECM; refs. 24–26), facilitating cancer cells to invade the stroma (4, 18). Macrophages are another important cell type in prostate cancer development, constituting 70% of the immune cell population in the prostate TME (27). Macrophages are attracted by cytokines released by prostate cancer cells and initially contribute to the immune defense against tumors (27). However, macrophages have a wide range of functions depending on environmental cues and can differentiate from a proinflammatory and anticancer (M1-type) to a procancer (M2-type) phenotype (28). The latter may support tumor cell proliferation, migration, and invasion (29, 30).

Although several studies have characterized developmental stages of prostate cancer and the underlying molecular mechanisms of tumorigenesis (12, 16, 28, 31–33), it is still unclear how such mechanisms jointly contribute to prostate cancer development (4).

Given the limitations of *in vivo* temporal data acquisition in studying heterogeneity at early stages in patients, novel models are required to study development of prostate cancer. Mathematical models offer valuable tools to study tumor development *in silico*. In particular, agent-based models (ABM) are spatial models that simulate the effect of interactions in complex multicellular systems such as tumors. This enables the investigation of how the overall system behavior originates from the interaction of individual components (34). In ABMs, cells are seen as agents that can interact with the surrounding cells (agents) based on a predefined set of rules. On the basis of stochastic simulations, ABMs enable monitoring the evolution of the tumor over time, and systematically test the impact of different aspects of the TME in a controlled way that would be unfeasible in any *in vitro* or *in vivo* settings (35).

Here we propose the first comprehensive ABM of prostate cancer onset and progression encompassing nine agent types and 60 parameters. Our model parameters are based on prior reports and in-house generated experimental data on LNCaP cultures and cocultures with fibroblasts, protumor, and antitumor macrophages. We show that our model reliably recapitulates different stages and spatial morphologies observed in cancer development, based on strong phenotypical parallels with histopathology images from patients with prostate cancer. In addition, we use the model to study which factors in the microenvironment mostly affect prostate cancer development, and to simulate *in silico* patients with different molecular characteristics, showing strong associations between *in silico* tumors and matching clinical data from The Cancer Genome Atlas (TCGA). We provide our ABM as a tool to systematically study the impact of the microenvironment on prostate cancer development.

Materials and Methods

Agent-based Modeling Assumptions and Simulations

In this study, we developed two ABMs to: (i) Test the requirements for prostate cancer tumor maintenance and (ii) Study the onset and progression of prostate cancer. In both cases, we used a two-dimensional (2D), on grid, stochastic ABM. The size of one grid space was set to the size of one tumor cell, 142.89 μm^2 (36) forming a 125×125 grid. The first model only includes tumor cells (normal and stem-like) and in all scenarios a total of 1,500 cells were randomly seeded. The second model includes nine different types of cellular agents (i.e., different *in silico* cell types) and cells were no longer seeded randomly, but in an ellipsoid geometry, mimicking the prostatic acinus. The average size of the lumen of the acinus was determined at 73 μm (six grid spaces; ref. 37) and increased to 156 μm (13 grid spaces), to adapt for the limitation that there are only two directions for growth and migration in the 2D model. Simulations were always repeated multiple times (as specified in the corresponding results sections) to account for the stochastic nature of ABM simulations.

Like all models, our models are an abstraction of reality and based on a set of assumptions which are listed in Supplementary Table S1. All agents (cells) occupy one space on the grid and compete for space in their Moore neighborhood (i.e., the eight surrounding grid spaces). The model iterates through a defined number of time steps. At each step, every agent can perform an action with a certain predefined probability. Unless specified otherwise in the following descriptions, all actions only affect agents (cells) in the Moore neighborhood. Probabilities of each action are defined by model parameters which are either derived from literature or estimated from our experimental data as detailed in the next sections. The complete list of model parameters is provided in Supplementary Table S2.

Modeling of Tumor Cells as Cellular Agents

In both models, tumor cell agents are seen as mutated luminal cells (normal or stem cells) and they have the possibility to acquire mutations (probability defined by the model parameter *TUpmut*; Supplementary Table S2) which confers them a proliferative advantage modeled as a (cumulative) increase in the probability of proliferation and maximum proliferation capacity (*TUadded values*; ref. 15). Mutated cells can migrate (*TUpmig*), die (*TUpdeath*), or proliferate (*TUpprol*). Cancer stem cells have the same characteristics as normal tumor cells, but they are additionally characterized by their self-renewal capacity (17). Therefore, stem cells are modeled as having infinite proliferation capacity, while other luminal cells have a limited proliferation capacity (*TUpmax*).

Implementation of an Agent-based Model of Prostate Cancer Onset and Progression

The more complex ABM that we developed to study prostate cancer development includes the tumor cells described in the previous section, and eight additional agents that can perform actions and interact with each other (Fig. 1). As stated above, this model's starting geometry mimics the one of a healthy prostate acinus, where luminal cells (including a fraction of stem cells) are placed on a layer of basal cells, which is attached to the basement membrane (11, 38). Luminal cells can acquire mutations and convert into tumor cells. A layer of tissue resident fibroblasts is placed outside of the acinus, surrounded by ECM containing more fibroblasts. Fibroblasts can convert to tumor-promoting CAFs when they are in proximity of tumor cells (18, 32, 39, 40). Macrophages can enter the simulation from the top left corner, simulating entry from a blood vessel. Although they exist in a broad spectrum, we consider a simplification of two phenotypes: M1 (immuno-promoting/antitumor) and M2 [tumor-promoting or tumor-associated macrophage (TAM)] macrophages (41).

In each iteration, all agents have their own round during which they can perform their actions or can idle based on the defined probabilities. The basement membrane and the ECM are instead passive agents that can only idle or be affected by the actions of other agents. Actions are performed by agents in the following order:

i. Luminal cells can proliferate (*LCpprol*) within their physiologic region and die (*LCpdeath*). They can also gain mutations (*TUpmut*), thereby converting into tumor cells (11). Mutations confer the cells a proliferative

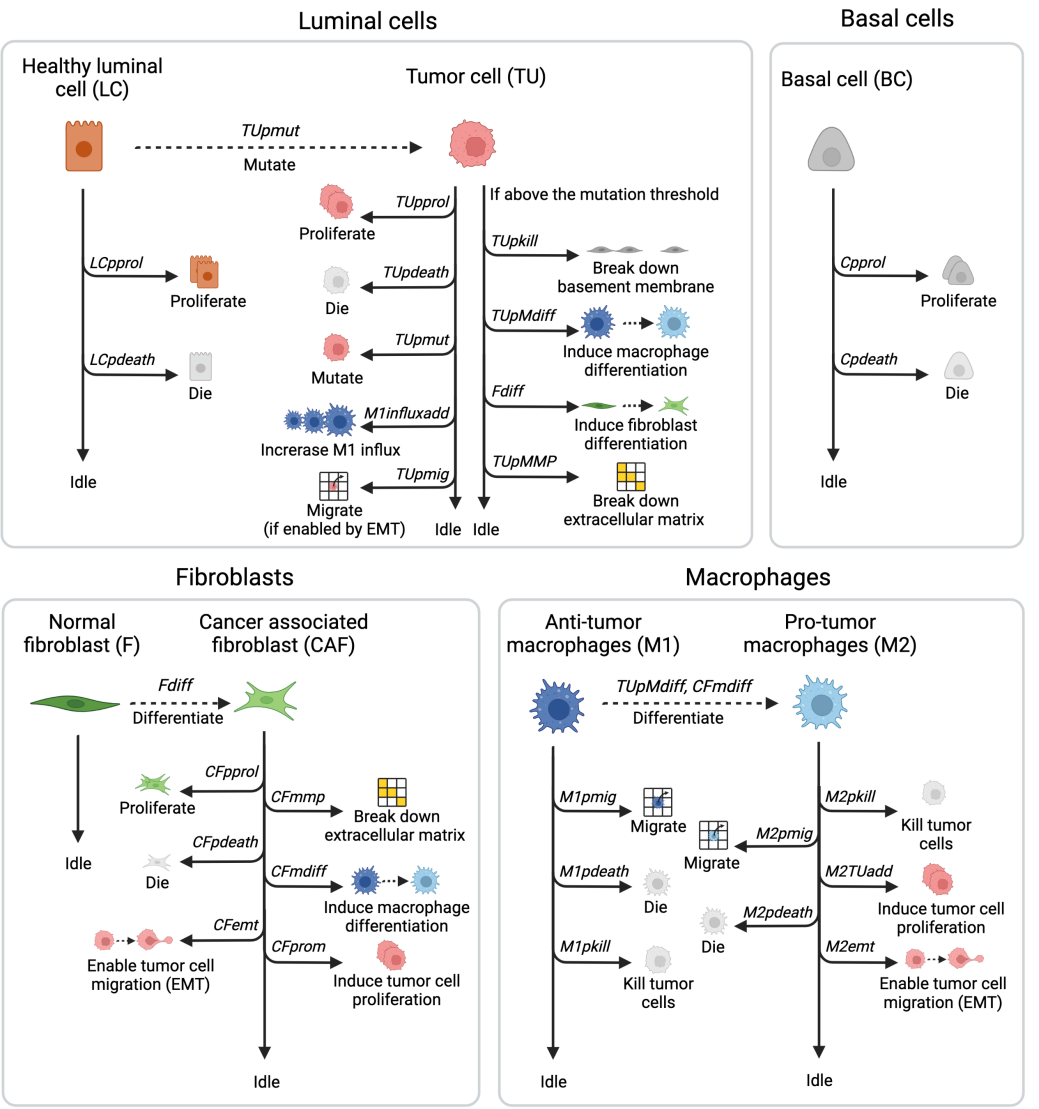

FIGURE 1 Overview of the agents and actions they can perform during each model iteration. The simulation starts with luminal cells (LC) and basal cells (BC) that can proliferate, die, or idle, all within physiologic regions and with fixed probabilities. The starting geometry also contains quiescent fibroblasts (F) and the passive agents (basement membrane and ECM), macrophages enter throughout the simulation. LCs can gain mutations, resulting in an increased M1-macrophage influx, once these mutated cells are sensed by macrophages. These mutated cells (TU) can additionally break down basement membrane and ECM and affect macrophage and fibroblast differentiation upon reaching mutation thresholds. Differentiated fibroblasts (CAF) proliferate, die, and can perform tumor-promoting actions. Just as the differentiated M2 macrophages, they stimulate TU proliferation and allow for TU migration. Macrophages (M1 and M2) can also kill tumor cells and die or migrate. Image created with BioRender.com.

advantage as well as an increased chance of gaining additional mutations. Tumor cells can die (*TUpdeath*), proliferate (*TUprol*) also outside their physiologic region, affect fibroblast differentiation (*Fdiff*) and increase macrophage influx (*M1influxadd*;refs. 30, 42). In addition, they can gain more mutations (*TUpmut*). Upon reaching mutation thresholds (*TUthrshBM*, *TUthrshM*, *TUthrshMMP*), tumor cells can perform additional actions: break down the basement membrane (*TUpkill*), affect macrophage differentiation (*TUpMdiff*), or break down the ECM (*TUpMMP*; refs. 38, 41, 43). After going through epithelial–mesenchymal transition (EMT), which is promoted by CAF or TAM proximity, tumor cells become invasive and can migrate randomly to an empty space in the Moore neighborhood (*TUpmig*; refs. 30, 44, 45).

ii. Basal cells can proliferate within their physiologic regions (*Cprol*) and die (*Cpdeath*). They must remain attached to the basement membrane to survive and cannot invade the lumen (38).

iii. Fibroblasts are quiescent, that is, they only idle (46). However, when they are in close proximity to tumor cells (i.e., maximum two grid spaces away, so the tumor cells can affect fibroblast differentiation over the basement membrane during PIN), they can differentiate into CAFs (*Fdiff*; ref. 47). CAFs can proliferate (*CFpprol*), die (*CFpdeath*), break down ECM (*CFmmp*), promote differentiation of macrophages toward the tumor-promoting phenotype (*CFmdiff*), enable migration for mutated cells (*CFemt*) and promote tumor cell proliferation (*CFprom*), by adding to the proliferation probability of tumor cells (21, 43, 44, 47).

iv. Macrophages can enter the simulation (*M1influxProb*), with an increased probability when macrophages detect tumor cells (*M1influxadd*; refs. 30, 42). All macrophages enter the simulation as M1 macrophages that can kill tumor cells (*M1pkill*), die (*M1pdeath*), or migrate (*M1pmig*). Macrophages move randomly, unless they can sense (within 17 grid spaces, to account for the effect of chemokines) tumor cells, as they will then move toward them (48, 49). When differentiated into tumor-promoting M2 macrophages, via stimulation by tumor cells or CAFs, they can additionally promote tumor cell proliferation (*M2TUadd*) and enable tumor cell migration (*M2emt;* ref. 30).

For typical simulations in this study, steps of 12 hours were used to simulate a period of 400 days. At each step, the model iterates through the rounds described above and each agent can perform one or more actions. Apart from stem cells, all other cells have a maximum number of times they can proliferate (luminal cells, tumor cells, basal cells, fibroblasts, and CAFs) or kill (macrophages) after which they get exhausted and die. Migration and proliferation can only occur in the standard Moore neighborhood, except for macrophages that can migrate in the Moore neighborhood of range 2 (24 neighbors instead of 8), to allow for acinus infiltration by traveling over the basement membrane (30, 42, 49).

Experimental Data for Parameter Estimation

We performed coculture *in vitro* experiments for fitting the model parameters. We used the prostate cancer cell line LNCaP (ATCC), immortalized foreskin fibroblast cells (BJ fibroblasts, Agami Lab NKI) and the monocytic cell line THP-1 (ATCC) which were differentiated into M1 or M2 macrophages. Cell lines were authenticated by short tandem repeat profiling (Eurofins; December 2022) and *Mycoplasma* testing was regularly performed by PCR every 3 months. Cells were kept at low passage (thawed at passage 2, used until maximum passage 8).

LNCaP cells and fibroblasts were cultured together with either M1- or M2-macrophages in a 4:1:1 ratio, respectively. Cells were cultured in physiologic hormonal conditions with R1881 used to induce androgen receptor (AR) signaling. LNCaP cells were tagged with eGFP to follow them overtime. LNCaP-eGFP cell proliferation was measured with IncuCyte Zoom fluorescent signal imaging system for 7 days and performed in triplicate. Finally, BJ fibroblast proliferation was measured separately by analysis of phase-contrast images from IncuCyte Zoom to obtain fibroblast growth curves, for fibroblast parameter determination.

Apoptosis was measured in real time using IncuCyte Zoom (Essen BioScience). To this end, cells were grown in FBS, including androgen, with an addition of Caspase-3/7 Read Reagent for Apoptosis (Essen Bioscience) in duplicate.

The resulting growth curves (Supplementary Fig. S1) and apoptosis data of prostate cancer cells were used to determine the parameters of tumor cells in the model.

Parameter Identification

Tumor cell, fibroblast, and macrophage parameters were estimated using particle swarm optimization to fit the experimental data (Supplementary Fig. S1). For each biological replicate, parameters were optimized 50 times to account for biological variation and model stochasticity. Final parameter values were fixed to the average estimated value after assessing the robustness of the estimated values between replicates. The optimizations were done sequentially, fixing the estimated model parameters. First, *TUpmax* and *TUpprol* were fitted to the experimental growth curves of the LNCaP cells. *TUpdeath* was determined by measuring apoptosis of LNCaP cells. Subsequently, *Fpprol*, *Fpmax*, and *Fpdeath* were fitted using the fibroblast growth curves. Finally, *M1pkill* and *M1kmax* were fitted using the experimentally obtained growth curve for tumor cells in the presence of M1 macrophages and fibroblasts. Similarly, *M2pkill was* determined. *M2kmax* was assumed equivalent to *M1kmax*.

The remaining parameter values were either derived from previous studies, adapted from a previously published model of colorectal cancer (49, 50) or qualitatively tuned (all details and specific references are in Supplementary Table S2).

Parameter Sensitivity Analysis

A qualitative sensitivity analysis was performed for all individual model parameters by increasing them individually by 10% and recording the percentage change in output, in the number of tumor cells at 400 days. All simulations were conducted 10 times to account for model stochasticity. Parameters with low sensitivity (i.e., for which the increase did not affect the output above the deviations due to the stochasticity of the model) were fixed and are specifically mentioned in Supplementary Table S2. Follow-up analyses were conducted for the four most sensitive parameters (i.e., those causing on average $>$ 10% change in output), simulating 10 intermediate values in the region of interest (i.e., in which the effect of changing the parameter is visible but not so extreme as to overpower all other parameters). Finally, pairwise combinations (with five parameter values each) of the most sensitive parameters were conducted to see whether there were synergistic or antagonistic relations. In all sensitivity analyses, the relative tumor size was recorded at 400 days and averaged across 10 simulations.

Pathology Slides for Assessment of Morphologic Features

Pathology slices of patients with prostate cancer were used, with permission, to compare growth patterns in patients with the model simulations. The patient samples were randomly picked out of daily practice of prostatectomies of patients with prostate cancer. Every slide consists of a 4-μm-thick section of formalin-fixed paraffin-embedded material and was stained with hematoxylin and eosin (H&E). The uropathologist scanned the slides and chose representative images of prostate carcinoma.

The use of patient archival prostatectomy materials for research purposes at the Netherlands Cancer Institute has been executed pursuant to Dutch legislation and international standards. Prior to May 25, 2018, national legislation on data protection applied, as well as the International Guideline on Good Clinical Practice. From May 25, 2018 on, we also adhere to the General Data Protection Regulation. Within this framework, patients are informed and have always had the opportunity to object or actively consent to the (continued) use of their personal data and biospecimens for research purposes. For the current study, written informed consent was obtained from all patients. Hence, the procedures comply both with (inter)national legislative and ethical standards.

Comparison Between Model Simulations and Clinical Patient Data

Model predictions were compared with clinical data from TCGA, using *in silico* generated tumor loads and clinical progression-free survival (PFS) time for comparison. Tumor load was defined as the amount of mutated cells at $t = 400$ days, for simulations that reached the cancer stage (breakdown of

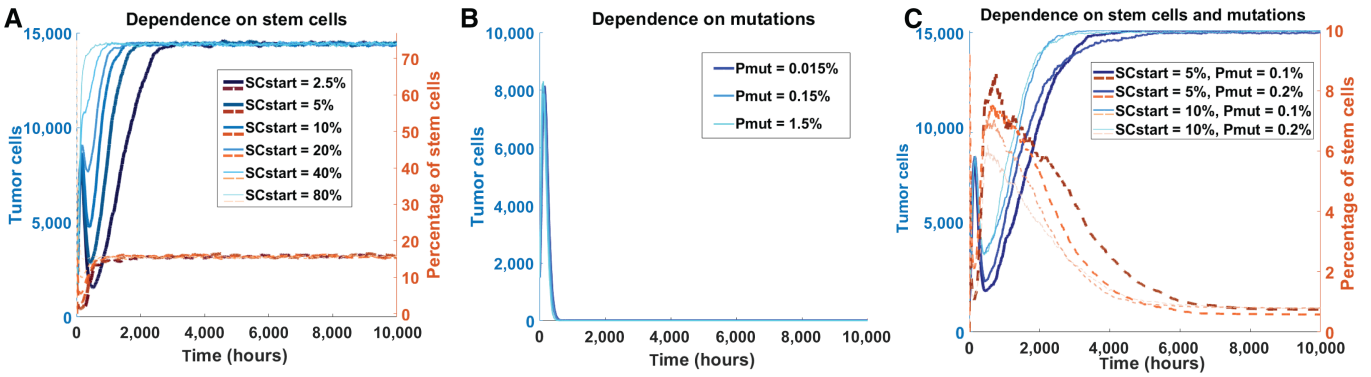

FIGURE 2 *In silico* testing of requirements for tumor maintenance. **A,** Amount of tumor cells (blue) and percentage of stem cells (orange, dotted) simulated over time under the condition that included only stem cells to maintain tumors. Simulations for six different initial percentages of stem cells (SCstart) are shown. **B,** Similar plot testing the condition in which the proliferative advantage of mutated tumor cells is the only source for tumor maintenance. Simulations for three different probabilities of acquiring mutations (Pmut) are shown. **C,** Similar plot testing the condition in which tumor maintenance depends on both stem cells and tumor cells that can gain mutations. Four combinations of initial stem cell percentage and probability of mutation acquisition are shown.

basement membrane). We used a cohort of $N = 494$ patients with prostate cancer for which molecular data (transcriptomics and genomics) and survival data (51) were available. RNA sequencing data were downloaded via the Firehose tool from the BROAD institute (released January 28, 2016) and processed as described by Lapuente-Santana and colleagues (52). To allow for comparison between expression levels of different genes, transcripts per million were used. Tumor mutational burden (TMB) data were obtained from a previous report (53). Quantifications of the relevant cell types for individual patients were obtained using deconvolution methods accessible through the *immunedeconv* R package (54): M1 and M2 macrophages were obtained using quanTIseq (55) and CAFs were derived using EPIC (56). Finally, for 333 patients with prostate cancer, we also retrieved information on Gleason score and binarized them as high (>7) and low (<7) Gleason score, thus excluding patients with intermediate-grade prostate cancer (Gleason score = 7; ref. 57). For the comparison of model simulations and clinical PFS, we performed correlation analysis (Spearman and Pearson), considering the PFS time as curated by Liu and colleagues (51) defined as the time to progression in case of events and the time to last contact or time to death in case of no event.

Computational Implementation

The ABM of prostate cancer onset and development is available as Matlab code in a GitHub repository at https://github.com/SysBioOncology/ABM_prostate_cancer_development.

Data Availability

Cell culture data are shown in the Supplementary Figures. Raw data are available from the corresponding authors upon request.

Results

In Silico Prostate Tumors Require a Proliferative Advantage of Mutated Cells Additionally to Cancer Stem Cells to Maintain Themselves at Realistic Stem Cell Percentages

Cancer stem cells are known to play an important role in prostate cancer development (17, 33, 58, 59, 60). To identify the percentage of stem cells needed for our *in silico* tumors to maintain themselves, we used a simple ABM including only normal tumor cells and/or tumor stem cells (as defined in Materials and Methods) that were randomly seeded on the grid to test different possible scenarios *in silico* (11). For the first scenario, tumor cells were not allowed to gain a proliferative advantage via mutations. This allowed us to assess the ability of stem cells alone to sustain the tumor. Irrespective of the starting percentage of stem cells, we achieved an almost full grid at approximately 15,000 tumor cells and stabilizing stem cell percentage at approximately 17% (Fig. 2A). While the tumor was able to survive with stem cells alone, this final stem cell percentage is much higher than we could reasonably expect based on literature, which is reported to be 0.1%–0.3% in the human prostate (33). The second scenario included no stem cells, but only tumor cells with a possibility of gaining (more) mutations that confers proliferative advantage. For all simulations, all tumor cells died within 40 days, meaning that a tumor cannot survive based on acquired mutations only, as the balance between cell proliferation and cell death eventually becomes negative as tumor cells get exhausted (Fig. 2B). The unlimited proliferative capacity of stem cells is needed as a source for new malignant cells. The third scenario included both a percentage of initial stem cells and tumor cells with the ability of gaining mutations. In this case, the tumor could maintain itself while the percentage of stem cells stabilized at a much lower value; approximately 0.5% (Fig. 2C). On the basis of these observations, we conclude that the combination of stem cells and possibility for luminal cells to mutate (and with that, gain a proliferative advantage), is required for tumor maintenance at realistic stem cell levels, and that this does not depend on the initial percentage of stem cells.

Model Simulations Recapitulate Known Steps of Prostate Cancer Development

After defining the basic requirements for tumor maintenance, we developed a comprehensive ABM to describe onset and development of prostate cancer in a simulated *in vivo* setting starting from a healthy prostate acinus (Fig. 3). This model is schematically depicted in Fig. 1 and is based on the set of assumptions and parameters described in Supplementary Tables S1 and S2, respectively (see Material and Methods).

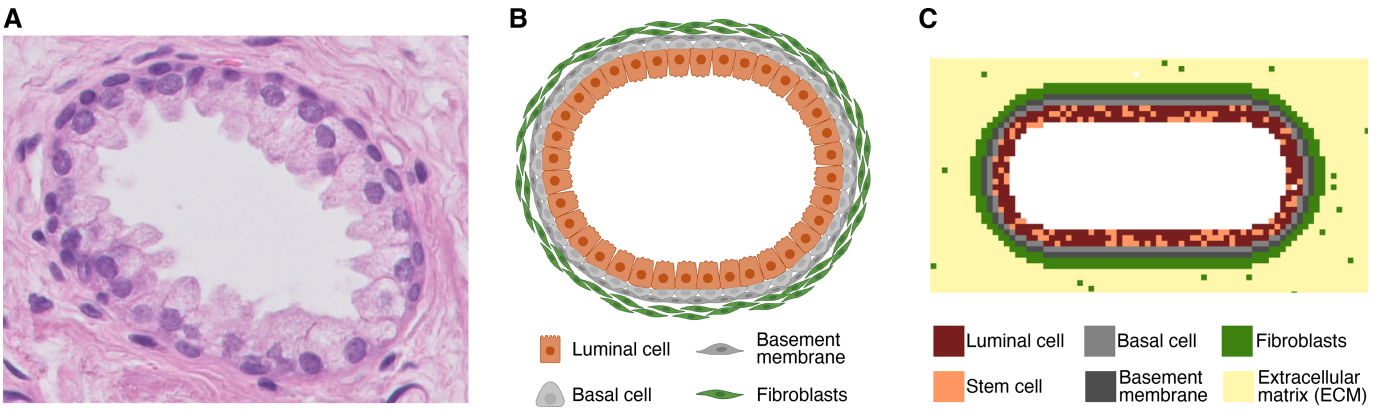

FIGURE 3 Overview of the starting geometry in 3-fold; a pathology slice, schematic representation, and model geometry visualization. **A,** A histology slice of a healthy prostatic acinus (H&E staining, 400x magnification). **B,** Schematic representation of the acinus (created with BioRender.com). **C,** Modeled starting geometry, including a color scheme of all cells included in the starting geometry.

Running the model simulations, we can observe how prostate cancer develops over time (Fig. 4A–I; Supplementary Video V1). The initial condition is a healthy prostatic acinus with empty lumen (Fig. 4A). Luminal cells can start to mutate and then grow in the lumen (Fig. 4B). Mutated luminal cells give rise to PIN, characterized by luminal cell hyperplasia, while the basement membrane remains intact (refs. 11, 61, 62; Fig. 4B–F). Mutated luminal cells (hereafter called tumor cells) attract macrophages, resulting in an increased macrophage influx toward the acinus (Fig. 4C; refs. 30, 41). Basal cell layer breakdown starts to occur during early PIN (Fig. 4D) and increases exponentially with disease progression (14). During prostate cancer development, CAFs originate from normal fibroblasts due to tumor cell stimulation (Fig. 4E; ref. 63). Tumor cells also affect polarization of macrophages toward the tumor-promoting phenotype by cytokine secretion, resulting in an increased number of M2-like macrophages (Fig. 4F). This increasing tumor-promoting environment results in basement membrane breakdown (Fig. 4G). This is a critical step as tumor cells are no longer confined in the acinus and they can invade the surrounding tissue allowing the disease to progress toward cancer. The tumor-promoting cells (TAMs and CAFs) elicit EMT in tumor cells, making them invasive (Fig. 4H; refs. 44, 45). This results in tumor cells invading the surrounding tissue, and thereby starting the cancerous phase (Fig. 4I). On the basis of these findings, we conclude that our model can represent all main steps of prostate cancer onset and development well.

Using the parameter set defined in Supplementary Table S2, we ran 500 simulations and observed that only 36% of them results in breaking down of the basement membrane, which we consider as a marker of invasive prostate cancer. We decided to investigate the main stochastic factors contributing to tumor development *in silico*. If the malignant cells are recognized by the M1 macrophages at an early stage, this results in a fast increase in the ratio of M1 macrophages to tumor cells. This allows the immune system to control and overcome the disease (Supplementary Fig. S2A). However, if this does not happen at early stages, the tumor develops to evade the immune response and subverts the immune response by converting macrophages to the protumor phenotype, increasing the M2:M1 macrophage ratio (Supplementary Fig. S2B). M2 macrophages can promote the tumor by increasing proliferation and eliciting EMT of mutated cells. We also observed that there are several factors that contribute to determining the time of invasion. Earlier invasions are characterized by higher numbers of CAFs, a higher average mutation load and higher M2:M1 macrophage ratio (Supplementary Fig. S2C–S2E). These results highlight how, based on stochastic simulations, our ABM enabled us to identify the aleatory factors that support prostate cancer development.

Model Simulations Recapitulate Geometries Present in Histology Images

Does our *in silico* prostate cancer model reliably represent clinically observed tumor growth patterns? To address this question, we compared our model simulations with pathology slides of patients with prostate cancer that were randomly picked out of daily practice. The uropathologist scanned the slides and selected representative images of prostate carcinoma. A common growth pattern during the PIN phase is tufting, which is characterized by protrusions consisting of multiple cell layers growing on the basal cell layer (ref. 64; Fig. 5A), which was observed as emergent behavior in our model simulations (Fig. 5B). In the simulations, this tufted geometry originates from mutated cells that grow in clusters attached to the basal cell layer. Interestingly, permanent "tufts" in our model contain stem cells suggesting that the presence of stem cell clusters could be an indication of the directionality of tumor growth. Another common growth pattern in developing prostate cancer is bridging, when cells grow from one side of the acinus toward the other side (Fig. 5C), which was also portrayed in the *in silico* developing tumors (Fig. 5D). Overall, we can conclude that our ABM recapitulates important growth patterns observed in histology slices of actual patients with prostate cancer.

Tumor Development is Most Strongly Impacted by Mutation Probability, Tumor-promoting Ability of CAFs, and Macrophage Phenotype

Having established that the simulated onset and development of prostate cancer recapitulates tumor developmental processes and growth patterns as observed in patients, we next investigated which model parameters most strongly affect tumor growth. Performing sensitivity analyses (Materials and Methods), we identified four model parameters causing a strong variation in the final simulated tumor load (Fig. 6A). These sensitive model parameters are: tumor promotion by CAFs (*CFprom*), migration probability of antitumor M1-like macrophages (*M1pmig*), tumor mutation load required for macrophage differentiation *(TUthrshM)*, and mutation probability for luminal cells (*TUpmut*). Looking at the dynamics of tumor formation when tuning these parameters, we observed that the mutation probability increases growth speed from the start of

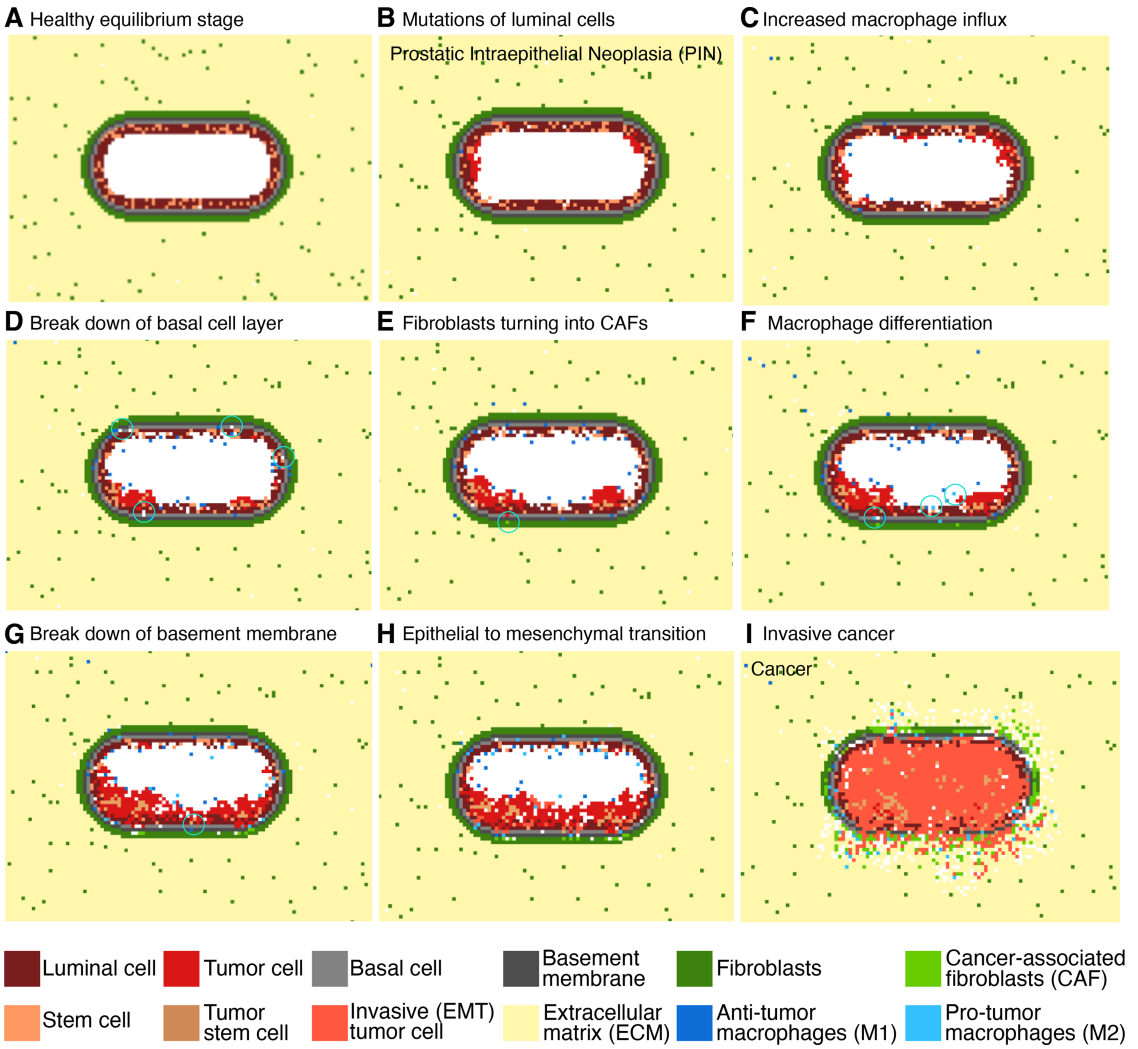

FIGURE 4 Initial healthy stage and following eight steps of prostate cancer development as by prostate cancer ABM simulation. **A,** Healthy prostatic acinus. **B,** Mutations start to occur in the luminal cells converting them into tumor cells. **C,** The presence of mutated cells increases the influx of M1 macrophages. **D,** Mutated cells start to occupy spaces in the basal cell layer. **E,** Fibroblasts are differentiating toward their tumor-promoting phenotype (CAFs). **F,** Macrophages are differentiating toward their tumor-promoting phenotype. **G,** All these factors lead to break down of the basement membrane. **H,** Mutated cells become more invasive and start undergoing EMT. **I,** Invasive cancer with cells spreading through the surrounding tissue. The white grid spaces indicate "empty space," corresponding to the lumen or to the cleaved ECM (e.g. by CAFs).

the simulation, while the protumorigenic effects of macrophage influx and CAF involvement occur at a later stage (Supplementary Fig. S3). Because these parameters can be related to molecular markers which are largely variable between patients, we decided to vary the corresponding parameters to generate relevant *in silico* patient populations. Analyzing the combined effect of parameter pairs on tumor growth, we empirically selected one high and one low value for each parameter (Supplementary Table S3). We chose values for which the effects of the parameter variation were clearly observable, but not too overpowering (other parameters having little/no effect based on Supplementary Fig. S4). To reduce the number of variables to have big enough clinical patient groups for the analysis described in the next section, we merged the two macrophage parameters: high migration probability and low threshold for phenotype switching (protumor macrophages) versus low migration probability and high threshold for macrophage phenotype switching (antitumor macrophages). This resulted in three parameter sets that allow for simulation of patients with: (i) High versus low level of tumor-promoting effect of CAFs; (ii) High versus low protumor macrophage characterization; (iii) High versus low level of mutation frequency of tumor cells. By systematically combining the effect of these three parameter sets, we obtained eight patient groups (Fig. 6).

For all four groups with high tumor mutation probability, over 88% of the simulations showed disease progression toward cancer (Supplementary Table S4). This is lower for other groups, with the two groups with protumor macrophages and low mutation probability resulting in modeled cancer progression in less than 8% of the simulations.

To compare model simulations with clinical data, which are only available for developed tumors from patients who underwent prostate surgery, we performed follow-up analysis considering only the simulations resulting in cancer development. The group with the most aggressive tumors consists of simulated patients with high tumor-promoting CAFs, high protumor macrophages

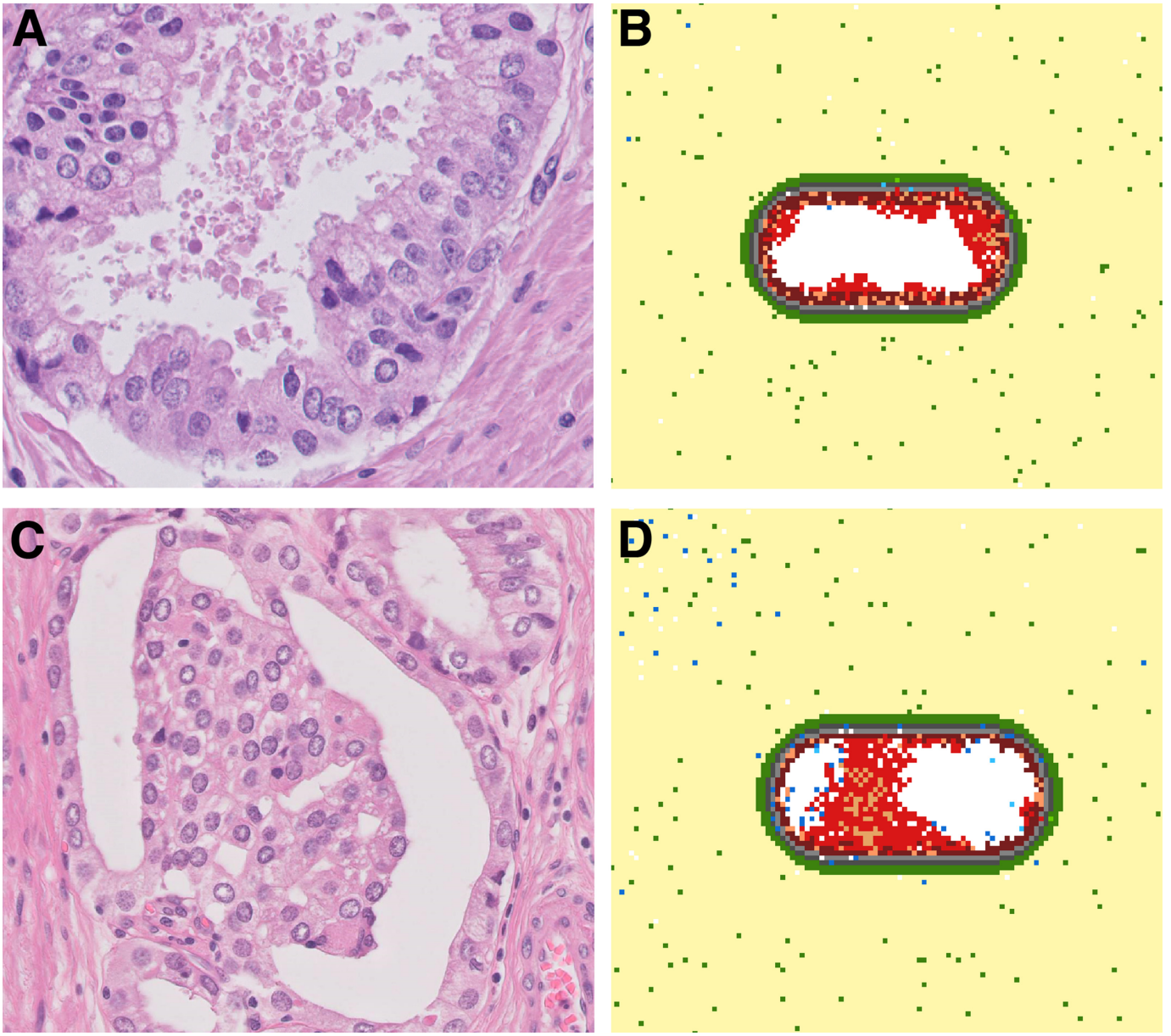

FIGURE 5 Comparison between model simulations and histology images (tufting and bridging). **A,** Pathology slice of a prostate cancer patient (H&E staining, 400x magnification) showing a "tufted" pattern of growths on the luminal cell layer. **B,** Model simulation depicting the tufting growth pattern. **C,** Pathology slice of a prostate cancer patient (H&E staining, 400x magnification) showing bridging; growth of cells from one side of the acinus toward the other side. **D,** Simulated prostate cancer development showing the bridging growth pattern.

characterization and a highly aggressive tumor cell phenotype (red line showing the simulated tumor growth over time in Fig. 6B and corresponding example simulation in the red box in Fig. 6C). On the contrary, the group with the least aggressive tumors is simulated when all parameter sets are set to "low" (i.e., the least tumor-promoting phenotype; pink line in Fig. 6B and pink box in Fig. 6C).

As expected, the time of invasiveness (i.e., breakdown of the basement membrane, marked with an x in Fig. 6B) is significantly earlier for the tumors with high mutation probability as compared with those with low mutation probability (one-sided Wilcoxon rank-sum test, $P = 2.26e\text{-}10$). However, the time of invasiveness does not always correlate with growth speed. The tumor group with the steepest growth curve (red line, Fig. 6B) becomes invasive later compared with more slowly growing tumors (e.g., the blue line, with antitumor macrophage characterization, $P = 0.030$). This analysis suggests that different mechanisms can affect how quickly tumors develop and how long it takes for tumors to become invasive.

Model Simulations of Tumor Load Associate with Patient Prognosis

Considering the same eight patient groups (all possible combinations of the three parameter sets) defined in the previous section, we wanted to assess whether the *in silico* behaviors correlate with patient prognosis. To do so,

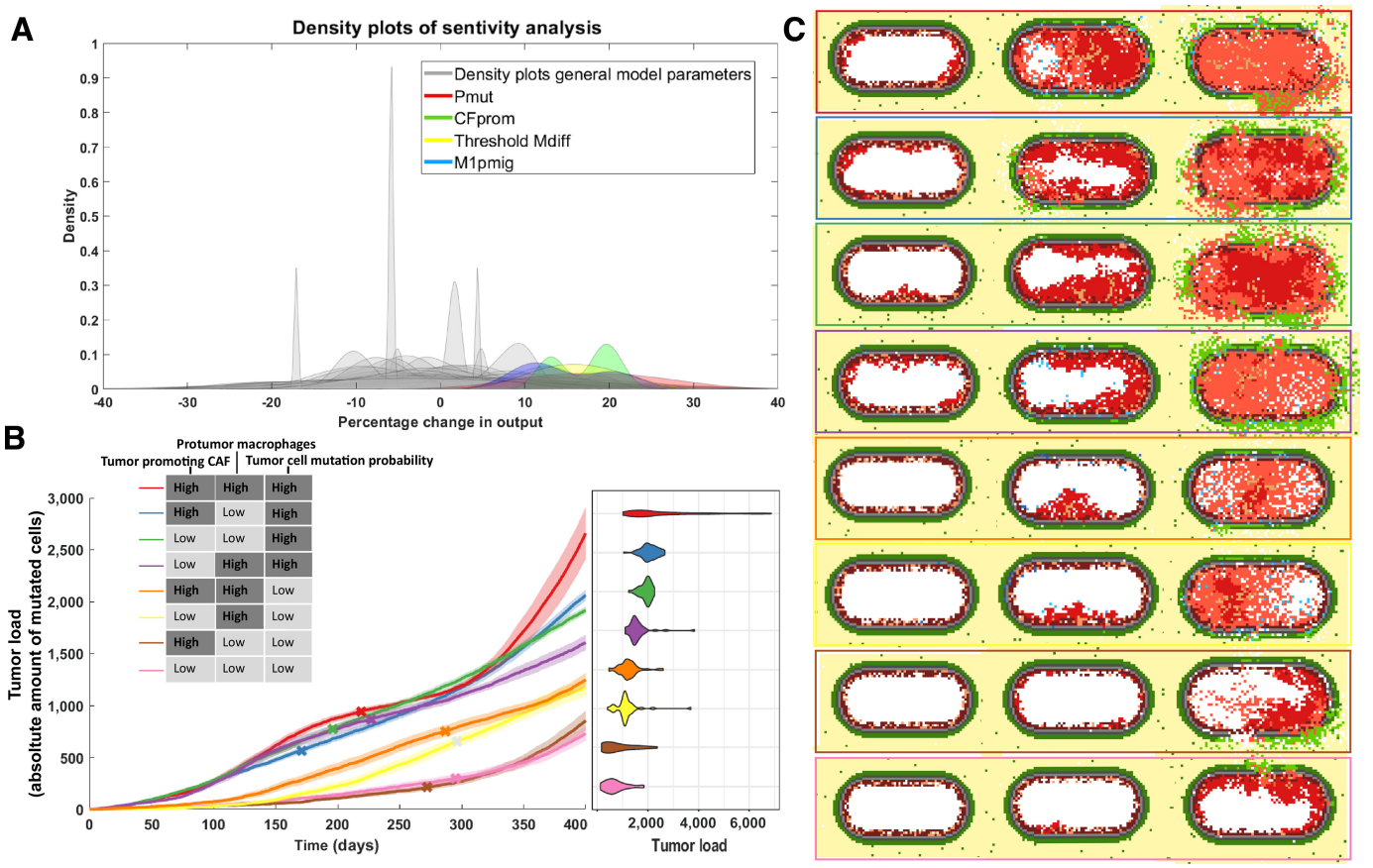

FIGURE 6 Effect on tumor growth of varying sensitive model parameters. **A,** Grouped histogram of the repeated sensitivity analysis (five times for each parameter), overlapped by four (differently colored) histograms of the most sensitive parameters: mutation probability of luminal cells (Pmut, red), probability of CAFs promoting tumor cell proliferation (CFprom, green), yellow represents the amount of mutations needed before tumor cells affect macrophage differentiation (TUthrshM) and M1 macrophage migration probability (M1pmig, blue). **B,** The averaged evolution of the amount of tumor cells for 40 simulations that developed cancer for each of the eight subclasses. These classes were based on the "high" or "low" status of sensitive parameters for CAFs, TAMs, and tumor cells. Included is a violin plot depicting the spread of simulated tumor cell amounts. **C,** An example of tumor development for each group at an early point in the simulation (50 days), the point at which it becomes invasive and the state at the end of the simulation (400 days).

we compared model predictions of tumor load (only for cases that developed cancer) with clinical data from a cohort of patients with prostate cancer ($N = 494$) from TCGA database. For each of the three parameter sets, we defined whether a patient belonged to the "low" or "high" group considering three molecular markers (see Supplementary Table S5 for detailed motivation of the choice of the markers). Tumor aggressiveness was defined on the basis of TMB and the expression of two frequently mutated genes in prostate cancer (*TP53* and *CDKN1B*; refs. 15, 65, 66). Protumor macrophage characterization was defined on the basis of the ratio of M2:M1 macrophages and the expression of two genes involved in protumor macrophage differentiation (*CXCL2* and *STAT3*; refs. 67–69). Finally, the tumor-promoting CAFs effect was defined on the basis of the quantification of CAFs and the expression of two soluble molecules secreted by CAFs that affect tumor progression (*TGFBR2* and *IGF1*; the latter one with an inverse relationship based on supporting literature and the negative correlation observed in our data; refs. 40, 70–72). For each parameter set, a patient was assigned to the "high" category if at least two out of three makers were above the cohort median, and "low" otherwise. We decided to use three markers to capture different aspects of the process described by the corresponding model parameters. For example, to assess tumor-promoting effects of CAFs, we considered not only the amount of CAFs (quantified using computational deconvolution) but also their ongoing differentiation and their tumor-promoting activity (using *TGFBR2* and *IGF1* as proxies respectively; more detailed justification is provided in Supplementary Table S5). In this way, we could divide TCGA patients in eight clinical patient groups with similar characteristics to the *in silico* groups.

We observed a negative correlation between the tumor load from the *in silico* patient groups and the PFS time of the matching clinical patients with prostate cancer. (Pearson correlation $= -0.73$, $P = 0.04$; Fig. 7A). Patients classified in the three groups with highest tumor load showed a significantly higher Gleason score (χ^2 test, $P = 0.002$; Fig. 7B) as compared with the patients in the three groups with lowest tumor load. Overall, these results indicate that tumors which are characterized to be more aggressive *in silico* correspond to patients with higher grade and worst prognosis.

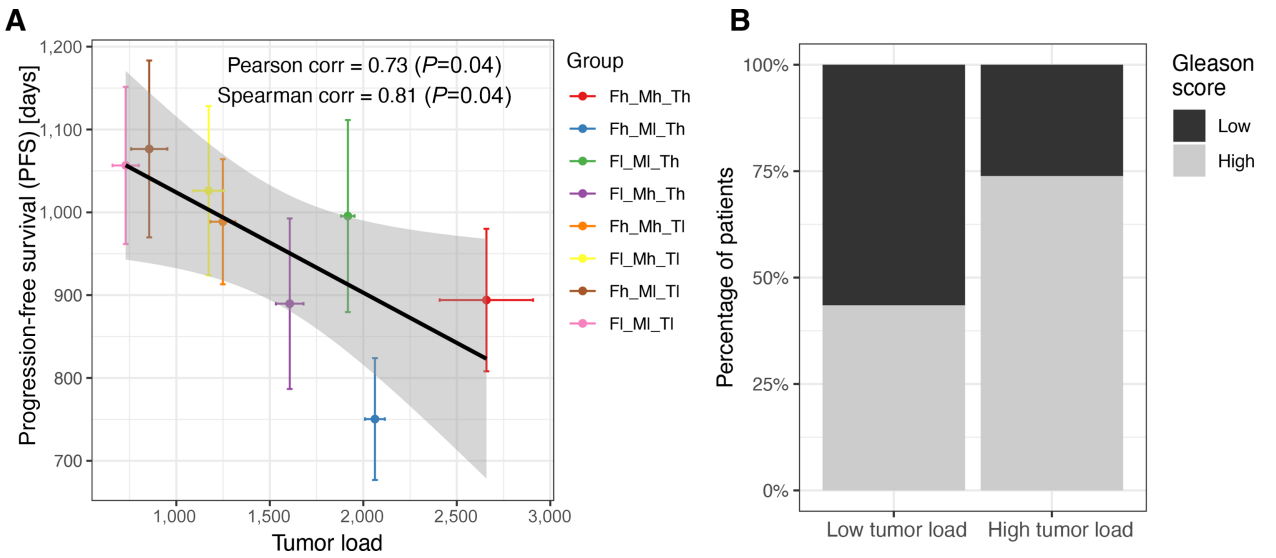

FIGURE 7 Clinical validation of model predictions for different patient groups. **A,** Correlation between the simulated tumor growth (simulation time 400 days, 40 simulations per modeled patient group) and the average PFS time for clinical patients assigned to the matching patients groups based on molecular markers. Colors correspond to those used in Fig. 6B, portraying simulated tumor growth over time of the same classes. **B,** Binary Gleason scores per patient group; Gleason scores of 8 or higher were considered "high" and Gleason scores of 6 or lower were considered "low".

Discussion

The process of prostate cancer development can take years and is heavily influenced by many different types of cells, stochastic events, and the TME. Its unpredictable nature and extensive adaptation strategies bear resemblance to the process of evolution, which makes it particularly hard to combat at a later stage. Recreating the complete disease settings to better understand and treat the disease is therefore rather difficult in *in vitro* or *in vivo* settings.

As recently emphasized in an opinion article by West and colleagues (73), agent-based models are key tools to reproduce the complexity of the tumor *in silico*, offering a complementary approach to *in vitro* and *in vivo* experiments. They allow the integration of different types of knowledge, framing it in the form of an intuitive set of rules. Despite their simplicity in the formulation, they allow simulation of complex behaviors deriving from cell–cell interactions.

Here, we designed a comprehensive agent-based model that provides an *in silico* experimental set up to study prostate cancer onset and progression. The rules defining our ABM were based on a set of assumptions integrating knowledge from several studies. Model parameters were additionally fine-tuned by fitting our in-house generated *in vitro* coculture data. After showing that our model was able to reproduce known tumor patterns and relevant steps of tumor progression, we used the model to *in silico* study the impact that deterministic and stochastic events have on prostate cancer progression.

In our study, we identified protumor activity of CAFs and macrophages and mutation probability of the tumors as main deterministic causes of *in silico* tumor heterogeneity. While high tumor mutation probability generally results in fast invasion and bigger tumors, the effects and quantities of macrophages and fibroblasts at different timepoints were found to be a very important factor in prostate cancer development and progression too. We suggest a different approach to classify patients based on functional TME characterization, thus providing a complementary view with respect to standard genomics-driven approaches (57). On the basis of our classification, we have shown that *in silico* progression correlates significantly with PFS, which is commonly used as a proxy of clinical progression although its validity has been challenged (74). Unfortunately, metastasis-free survival, which is the most reliable clinical indicator, is not available for most publicly available datasets. Our results represent a proof of principle that our model could help to improve our understanding of different patient molecular characteristics and how these contribute to the likelihood of progression, thus suggesting new prevention strategies and options for patient-tailored treatment plans. However, more clinical data on patients not (yet) in a malignant disease stage and more informative clinical endpoints would be needed to assess whether these markers could be used as indicators of disease stages and be functionally associated with disease progression. This assessment could be tested by monitoring prostatitis patients, which is a risk factor for prostate cancer (75).

We additionally observed that, running the model multiple times starting with the same initial conditions, only a fraction of the simulations developed into cancer. This is determined only by the stochasticity of the events included in the simulation that mimics the *in vivo* stochasticity of cellular interactions. We observed that aleatory events related to the interactions between macrophages and tumor cells can determine the success of early immunosurveillance thus determining the fate of the tumor. The stochasticity of interactions also affects how long it takes before the tumor becomes invasive, driven by the balance between the number of CAFs, amount of driver mutations and the ratio of antitumor/protumor macrophages. While there is increasing awareness that clinicians should consider the impact of genetics to account for patients heterogeneity in prostate cancer management (76, 77), our results underlie the importance of monitoring the microenvironment phenotype (e.g., using multiplexed tissue imaging) during prostate cancer progression.

Although we have shown that our ABM is a valuable tool to conduct *in silico* experiments on the onset of prostate cancer, it is important to keep in mind that models are always an approximation of reality and the choice of the level of details included is driven by the aim of the study. A limitation of the current study

is that the initial model parameters are based on experiments performed on a single prostate cancer cell line (LNCaP). While the systematic effect of cell line and patient heterogeneity, for example, due to differences in mutations, is captured by our sensitivity analysis on the model parameters, more experiments on different cell lines would be needed to further study differences in the trajectories and the stochastic events of prostate cancer development. On the basis of experiments with castration-resistant cell lines, our model could be extended in the future to study treatment response and more advanced disease stages, such as the effect of androgen deprivation therapy or AR inhibition and the development of castration resistance. Considering that AR is known to play a role, not only on prostate cancer cells, but also on fibroblasts (22) and macrophages (45), an extension of our ABM could be a valuable tool to take an integrative approach to study how the prostate cancer microenvironment mediates therapy response.

In addition, for this study, we chose to focus on macrophages and fibroblasts because of their prominent role in prostate cancer, but the model could be further extended to include other cell types, such as T cells. Although prostate cancer is known to be an immune excluded and suppressed tumor type, recent studies showed the potential of combining T cell–based immunotherapies (i.e., immune checkpoint blockers or chimeric antigen receptor T cells) with other therapies targeting the prostate cancer microenvironment to restore antitumor immunity in advanced prostate cancer (78, 79). ABMs could help to understand the effect of combining different therapies in specific microenvironment subtypes, therefore suggesting how to tailor combinatorial treatment.

Furthermore, we have now chosen to model the effect of cytokines and chemokines implicitly (e.g., by basing an interaction between two cells on the distance between them), but it would be an interesting addition to model humoral factors explicitly [e.g., using hybrid models (80)], for example when wanting to zoom in more on androgen dependence and the path to castration-resistant disease. Adding to this, we have chosen to model mutations generally; all mutations confer a proliferative advantage and increased mutation chance to its host. An interesting addition to the model might be the explicit inclusion of the most common genomic alterations, such as *TMPRSS2-ERG* gene fusion (81). These additions would make the model more realistic but also more complex, thus increasing the number of model parameters and the computational costs.

Previous *in silico* models of prostate cancer have been focused on specific mechanisms such as the formation of bone metastases (62) or the role of disrupted stem cell movement in causing excessive growth in healthy prostatic ducts (82). To our knowledge, this is the first ABM to simulate the onset and development of prostate cancer in healthy prostatic acini considering the effects of the microenvironment including fibroblasts and macrophages. Our analysis shows that, not only tumor cells, but also macrophages and fibroblasts play an important role in prostate cancer development and could provide potential markers of disease progression.

Authors' Disclosures

W. Zwart reports grants from Astellas Pharma outside the submitted work. No disclosures were reported by the other authors.

Authors' Contributions

M. Passier: Conceptualization, software, formal analysis, visualization, methodology, writing-original draft. **M.N.G. van Genderen:** Software, formal analysis, visualization, writing-review and editing. **A. Zaalberg:** Validation, investigation, writing-review and editing. **J. Kneppers:** Validation, investigation, writing-review and editing. **E.M. Bekers:** Resources, validation, writing-review and editing. **A.M. Bergman:** Conceptualization, resources, supervision, writing-review and editing. **W. Zwart:** Conceptualization, resources, supervision, writing-review and editing. **F. Eduati:** Conceptualization, formal analysis, supervision, writing-original draft.

Acknowledgments

The results shown here are in part based upon data generated by TCGA Research Network: http://cancergenome.nih.gov/. The authors would like to thank Oscar Lapuente-Santana for providing the preprocessed TCGA data, Dr. F. Finotello for assistance in running the *immunedeconv* package and J. van Leeuwen for testing the code of the ABM. We would like to thank members of the Eduati, Zwart, and Bergman labs for valuable discussion and feedback.

Note

Supplementary data for this article are available at Cancer Research Communications Online (https://aacrjournals.org/cancerrescommun/).

Received February 24, 2023; revised May 15, 2023; accepted July 10, 2023; published first August 07, 2023.

References

1. Sung H, Ferlay J, Siegel RL, Laversanne M, Soerjomataram I, Jemal A, et al. Global cancer statistics 2020: GLOBOCAN estimates of incidence and mortality worldwide for 36 cancers in 185 countries. CA Cancer J Clin 2021;71: 209-49.
2. Ramon J, Denis LJ. Prostate cancer. New York (NY): Springer Science & Business Media; 2007.
3. Davidson D, Bostwick DG, Qian J, Wollan PC, Oesterling JE, Rudders RA, et al. Prostatic intraepithelial neoplasia is a risk factor for adenocarcinoma: predictive accuracy in needle biopsies. J Urol 1995;154: 1295-9.
4. Fahmy O, Alhakamy NA, Rizg WY, Bagalagel A, Alamoudi AJ, Aldawsari HM, et al. Updates on molecular and biochemical development and progression of prostate cancer. J Clin Med Res 2021;10: 5127.
5. Wang G, Zhao D, Spring DJ, DePinho RA. Genetics and biology of prostate cancer. Genes Dev 2018;32: 1105-40.
6. Germann M, Wetterwald A, Guzmán-Ramirez N, van der Pluijm G, Culig Z, Cecchini MG, et al. Stem-like cells with luminal progenitor phenotype survive castration in human prostate cancer. Stem Cells 2012;30: 1076-86.
7. Menon R, Deng M, Rüenauver K, Queisser A, Peifer M, Pfeifer M, et al. Somatic copy number alterations by whole-exome sequencing implicates YWHAZ and PTK2 in castration-resistant prostate cancer. J Pathol 2013;231: 505-16.
8. Grasso CS, Wu Y-M, Robinson DR, Cao X, Dhanasekaran SM, Khan AP, et al. The mutational landscape of lethal castration-resistant prostate cancer. Nature 2012;487: 239-43.
9. Gao H, Ouyang X, Banach-Petrosky WA, Shen MM, Abate-Shen C. Emergence of androgen independence at early stages of prostate cancer progression in Nkx3.1; Pten mice. Cancer Res 2006;66: 7929-33.

10. Glinsky GV, Glinskii AB, Stephenson AJ, Hoffman RM, Gerald WL. Gene expression profiling predicts clinical outcome of prostate cancer. J Clin Invest 2004;113: 913-23.
11. Packer JR, Maitland NJ. The molecular and cellular origin of human prostate cancer. Biochim Biophys Acta 2016;1863: 1238-60.
12. De Marzo AM, Platz EA, Sutcliffe S, Xu J, Grönberg H, Drake CG, et al. Inflammation in prostate carcinogenesis. Nat Rev Cancer 2007;7: 256-69.
13. Bostwick DG, Amin MB, Dundore P, Marsh W, Schultz DS. Architectural patterns of high-grade prostatic intraepithelial neoplasia. Hum Pathol 1993;24: 298-310.
14. Bostwick DG, Brawer MK. Prostatic intra-epithelial neoplasia and early invasion in prostate cancer. Cancer 1987;59: 788-94.
15. Barbieri CE, Baca SC, Lawrence MS, Demichelis F, Blattner M, Theurillat J-P, et al. Exome sequencing identifies recurrent SPOP, FOXA1 and MED12 mutations in prostate cancer. Nat Genet 2012;44: 685-9.
16. Alberts B, Johnson A, Lewis J, Raff M, Roberts K, Walter P. Molecular biology of the cell 6th ed. New York, NY: Garland Science; 2015.
17. Skvortsov S, Skvortsova I-I, Tang DG, Dubrovska A. Concise review: prostate cancer stem cells: current understanding. Stem Cells 2018;36: 1457-74.
18. Bonollo F, Thalmann GN, Kruithof-de Julio M, Karkampouna S. The role of cancer-associated fibroblasts in prostate cancer tumorigenesis. Cancers 2020;12: 1887.
19. Brizzi MF, Tarone G, Defilippi P. Extracellular matrix, integrins, and growth factors as tailors of the stem cell niche. Curr Opin Cell Biol 2012;24: 645-51.
20. Levesque C, Nelson PS. Cellular constituents of the prostate stroma: key contributors to prostate cancer progression and therapy resistance. Cold Spring Harb Perspect Med 2018;8: a030510.
21. Linxweiler J, Hajili T, Körbel C, Berchem C, Zeuschner P, Müller A, et al. Cancer-associated fibroblasts stimulate primary tumor growth and metastatic spread in an orthotopic prostate cancer xenograft model. Sci Rep 2020;10: 12575.
22. Cioni B, Nevedomskaya E, Melis MHM, van Burgsteden J, Stelloo S, Hodel E, et al. Loss of androgen receptor signaling in prostate cancer-associated fibroblasts (CAFs) promotes CCL2- and CXCL8-mediated cancer cell migration. Mol Oncol 2018;12: 1308-23.
23. Sun D-Y, Wu J-Q, He Z-H, He M-F, Sun H-B. Cancer-associated fibroblast regulate proliferation and migration of prostate cancer cells through TGF-β signaling pathway. Life Sci 2019;235: 116791.
24. Hynes RO. The extracellular matrix: not just pretty fibrils. Science 2009;326: 1216-9.
25. Roy R, Yang J, Moses MA. Matrix metalloproteinases as novel biomarkers and potential therapeutic targets in human cancer. J Clin Oncol 2009;27: 5287-97.
26. Cirri P, Chiarugi P. Cancer-associated-fibroblasts and tumour cells: a diabolic liaison driving cancer progression. Cancer Metastasis Rev 2012;31: 195-208.
27. Jeong S-H, Kwak C. Immunotherapy for prostate cancer: Requirements for a successful regime transfer. Investig Clin Urol 2022;63: 3-13.
28. Roca H, Varsos ZS, Sud S, Craig MJ, Ying C, Pienta KJ. CCL2 and interleukin-6 promote survival of human CD11b peripheral blood mononuclear cells and induce M2-type macrophage polarization. J Biol Chem 2009;284: 34342-54.
29. Martori C, Sanchez-Moral L, Paul T, Pardo JC, Font A, de Porras VR, et al. Macrophages as a therapeutic target in metastatic prostate cancer: a way to overcome immunotherapy resistance?. Cancers 2022;14: 440.
30. Thomas MU, Messex JK, Dang T, Abdulkadir SA, Jorcyk CL, Liou G-Y. Macrophages expedite cell proliferation of prostate intraepithelial neoplasia through their downstream target ERK. FEBS J 2021;288: 1871-86.
31. Pencik J, Schlederer M, Gruber W, Unger C, Walker SM, Chalaris A, et al. STAT3 regulated ARF expression suppresses prostate cancer metastasis. Nat Commun 2015;6: 7736.
32. Tuxhorn JA, Ayala GE, Smith MJ, Smith VC, Dang TD, Rowley DR. Reactive stroma in human prostate cancer: induction of myofibroblast phenotype and extracellular matrix remodeling. Clin Cancer Res 2002;8: 2912-23.
33. Collins AT, Berry PA, Hyde C, Stower MJ, Maitland NJ. Prospective identification of tumorigenic prostate cancer stem cells. Cancer Res 2005;65: 10946-51.
34. Wang Z, Butner JD, Kerketta R, Cristini V, Deisboeck TS. Simulating cancer growth with multiscale agent-based modeling. Semin Cancer Biol 2015;30: 70-8.
35. Norton K-A, Gong C, Jamalian S, Popel AS. Multiscale agent-based and hybrid modeling of the tumor immune microenvironment. Processes 2019;7: 37.
36. Lazar DC, Cho EH, Luttgen MS, Metzner TJ, Uson ML, Torrey M, et al. Cytometric comparisons between circulating tumor cells from prostate cancer patients and the prostate-tumor-derived LNCaP cell line. Phys Biol 2012;9: 016002.
37. Robinson S. Prostate volume, size does matter: growth dynamics of the acini and the stroma using a "Prostatocrit" model. SM J Urol 2018;4: 1037.
38. Liu A, Wei L, Gardner WA, Deng C-X, Man Y-G. Correlated alterations in prostate basal cell layer and basement membrane. Int J Biol Sci 2009;5: 276-85.
39. Ojalill M, Virtanen N, Rappu P, Siljamäki E, Taimen P, Heino J. Interaction between prostate cancer cells and prostate fibroblasts promotes accumulation and proteolytic processing of basement membrane proteins. Prostate 2020;80: 715-26.
40. Farhood B, Najafi M, Mortezaee K. Cancer-associated fibroblasts: secretions, interactions, and therapy. J Cell Biochem 2019;120: 2791-800.
41. Cess CG, Finley SD. Multi-scale modeling of macrophage-T cell interactions within the tumor microenvironment. PLoS Comput Biol 2020;16: e1008519.
42. Fang L-Y, Izumi K, Lai K-P, Liang L, Li L, Miyamoto H, et al. Infiltrating macrophages promote prostate tumorigenesis via modulating androgen receptor-mediated CCL4-STAT3 signaling. Cancer Res 2013;73: 5633-46.
43. Winkler J, Abisoye-Ogunniyan A, Metcalf KJ, Werb Z. Concepts of extracellular matrix remodelling in tumour progression and metastasis. Nat Commun 2020;11: 5120.
44. Giannoni E, Bianchini F, Masieri L, Serni S, Torre E, Calorini L, et al. Reciprocal activation of prostate cancer cells and cancer-associated fibroblasts stimulates epithelial-mesenchymal transition and cancer stemness. Cancer Res 2010;70: 6945-56.
45. Cioni B, Zaalberg A, van Beijnum JR, Melis MHM, van Burgsteden J, Muraro MJ, et al. Androgen receptor signalling in macrophages promotes TREM-1-mediated prostate cancer cell line migration and invasion. Nat Commun 2020;11: 4498.
46. Kalluri R. The biology and function of fibroblasts in cancer. Nat Rev Cancer 2016;16: 582-98.
47. Ghajar CM, Correia AL, Bissell MJ. The role of the microenvironment in tumor initiation, progression, and metastasis. Mendelsohn J, Gray JW, Howley PM, Israel MA, Thompson CB, Saunders WB, editors. The molecular basis of cancer 2014. p. 239-56.
48. Norton K-A, Jin K, Popel AS. Modeling triple-negative breast cancer heterogeneity: effects of stromal macrophages, fibroblasts and tumor vasculature. J Theor Biol 2018;452: 56-68.
49. Kather JN, Poleszczuk J, Suarez-Carmona M, Krisam J, Charoentong P, Valous NA, et al. In *silico* modeling of immunotherapy and stroma-targeting therapies in human colorectal cancer. Cancer Res 2017;77: 6442-52.
50. Kather JN, Charoentong P, Suarez-Carmona M, Herpel E, Klupp F, Ulrich A, et al. High-throughput screening of combinatorial immunotherapies with patient-specific models of metastatic colorectal cancer. Cancer Res 2018;78: 5155-63.
51. Liu J, Lichtenberg T, Hoadley KA, Poisson LM, Lazar AJ, Cherniack AD, et al. An integrated TCGA pan-cancer clinical data resource to drive high-quality survival outcome analytics. Cell 2018;173: 400-16.
52. Lapuente-Santana Ó, van Genderen M, Hilbers PAJ, Finotello F, Eduati F. Interpretable systems biomarkers predict response to immune-checkpoint inhibitors. Patterns 2021;2: 100293.
53. Thorsson V, Gibbs DL, Brown SD, Wolf D, Bortone DS, Ou Yang T-H, et al. The immune landscape of cancer. Immunity 2018;48: 812-30.
54. Sturm G, Finotello F, Petitprez F, Zhang JD, Baumbach J, Fridman WH, et al. Comprehensive evaluation of transcriptome-based cell-type quantification methods for immuno-oncology. Bioinformatics 2019;35: i436-45.
55. Finotello F, Mayer C, Plattner C, Laschober G, Rieder D, Hackl H, et al. Correction to: Molecular and pharmacological modulators of the tumor immune contexture revealed by deconvolution of RNA-seq data. Genome Med 2019;11: 50.
56. Racle J, de Jonge K, Baumgaertner P, Speiser DE, Gfeller D. Simultaneous enumeration of cancer and immune cell types from bulk tumor gene expression data. Elife 2017;6: e26476.
57. Cancer Genome Atlas Research Network. The molecular taxonomy of primary prostate cancer. Cell 2015;163: 1011-25.

58. Norton K-A, Popel AS. An agent-based model of cancer stem cell initiated avascular tumour growth and metastasis: the effect of seeding frequency and location. J R Soc Interface 2014;11: 20140640.
59. Zhang K, Guo Y, Wang X, Zhao H, Ji Z, Cheng C, et al. WNT/β-catenin directs self-renewal symmetric cell division of hTERT prostate cancer stem cells. Cancer Res 2017;77: 2534-47.
60. Zhou J, Wang H, Cannon V, Wolcott KM, Song H, Yates C. Side population rather than CD133 cells distinguishes enriched tumorigenicity in hTERT-immortalized primary prostate cancer cells. Mol Cancer 2011;10: 112.
61. Montironi R, Mazzucchelli R, Lopez-Beltran A, Cheng L, Scarpelli M. Mechanisms of disease: high-grade prostatic intraepithelial neoplasia and other proposed preneoplastic lesions in the prostate. Nat Clin Pract Urol 2007;4: 321-32.
62. Casarin S, Dondossola E. An agent-based model of prostate cancer bone metastasis progression and response to Radium223. BMC Cancer 2020;20: 605.
63. Anderberg C, Pietras K. On the origin of cancer-associated fibroblasts. Cell Cycle 2009;8: 1461-2.
64. Brawer MK. Prostatic intraepithelial neoplasia: an overview. Rev Urol 2005;7: S11-8.
65. Lynch SM, McKenna MM, Walsh CP, McKenna DJ. miR-24 regulates CDKN1B/p27 expression in prostate cancer. Prostate 2016;76: 637-48.
66. Xu J, Langefeld CD, Zheng SL, Gillanders EM, Chang B-L, Isaacs SD, et al. Interaction effect of PTEN and CDKN1B chromosomal regions on prostate cancer linkage. Hum Genet 2004;115: 255-62.
67. Di Mitri D, Mirenda M, Vasilevska J, Calcinotto A, Delaleu N, Revandkar A, et al. Re-education of tumor-associated macrophages by CXCR2 blockade drives senescence and tumor inhibition in advanced prostate cancer. Cell Rep 2019;28: 2156-68.
68. Kumar V, Cheng P, Condamine T, Mony S, Languino LR, McCaffrey JC, et al. CD45 phosphatase inhibits STAT3 transcription factor activity in myeloid cells and promotes tumor-associated macrophage differentiation. Immunity 2016;44: 303-15.
69. Nagarsheth N, Wicha MS, Zou W. Chemokines in the cancer microenvironment and their relevance in cancer immunotherapy. Nat Rev Immunol 2017;17: 559-72.
70. Soulitzis N, Karyotis I, Delakas D, Spandidos DA. Expression analysis of peptide growth factors VEGF, FGF2, TGFB1, EGF and IGF1 in prostate cancer and benign prostatic hyperplasia. Int J Oncol 2006;29: 305-14.
71. Franco OE, Shaw AK, Strand DW, Hayward SW. Cancer associated fibroblasts in cancer pathogenesis. Semin Cell Dev Biol 2010;21: 33-9.
72. Zhu M-L, Kyprianou N. Androgen receptor and growth factor signaling cross-talk in prostate cancer cells. Endocr Relat Cancer 2008;15: 841-9.
73. West J, Robertson-Tessi M, Anderson ARA. Agent-based methods facilitate integrative science in cancer. Trends Cell Biol 2023;33: 300-11.
74. Gharzai LA, Jiang R, Wallington D, Jones G, Birer S, Jairath N, et al. Intermediate clinical endpoints for surrogacy in localised prostate cancer: an aggregate meta-analysis. Lancet Oncol 2021;22: 402-10.
75. Dennis LK, Lynch CF, Torner JC. Epidemiologic association between prostatitis and prostate cancer. Urology 2002;60: 78-83.
76. Giri VN, Morgan TM, Morris DS, Berchuck JE, Hyatt C, Taplin M-E. Genetic testing in prostate cancer management: considerations informing primary care. CA Cancer J Clin 2022;72: 360-71.
77. Fontana F, Anselmi M, Limonta P. Molecular mechanisms and genetic alterations in prostate cancer: from diagnosis to targeted therapy. Cancer Lett 2022;534: 215619.
78. Narayan V, Barber-Rotenberg JS, Jung I-Y, Lacey SF, Rech AJ, Davis MM, et al. PSMA-targeting TGFβ-insensitive armored CAR T cells in metastatic castration-resistant prostate cancer: a phase 1 trial. Nat Med 2022;28: 724-34.
79. Peng S, Hu P, Xiao Y-T, Lu W, Guo D, Hu S, et al. Single-cell analysis reveals EP4 as a target for restoring T-cell infiltration and sensitizing prostate cancer to immunotherapy. Clin Cancer Res 2022;28: 552-67.
80. Cesaro G, Milia M, Baruzzo G, Finco G, Morandini F, Lazzarini A, et al. MAST: a hybrid multi-agent spatio-temporal model of tumor microenvironment informed using a data-driven approach. Bioinform Adv 2022;2: vbac092.
81. Adamo P, Ladomery MR. The oncogene ERG: a key factor in prostate cancer. Oncogene 2016;35: 403-14.
82. Lao BJ, Kamei DT. Investigation of cellular movement in the prostate epithelium using an agent-based model. J Theor Biol 2008;250: 642-54.